NAG3-507

LEWIS GRANT

IN-44-CR

103480

p.42

MODELLING OF MULTIJUNCTION CASCADE PHOTOVOLTAICS FOR SPACE APPLICATIONS

BY

JAMES LOUIS EDUCATO

B.S., University of Notre Dame, 1985

THESIS

Submitted in partial fulfillment of the requirements
for the degree of Master of Science in Electrical Engineering
in the Graduate College of the
University of Illinois at Urbana-Champaign, 1988

Urbana, Illinois

(NASA-CR-181417) MODELLING OF MULTIJUNCTION CASCADE PHOTOVOLTAICS FOR SPACE APPLICATIONS M.S. Thesis, 1988 (Illinois Univ.) 42 p Avail: NTIS HC A03/MF A01 CSCL 10A

N87-29958

Unclas

G3/44 0103480

MODELLING OF MULTIJUNCTION CASCADE PHOTOVOLTAICS FOR SPACE APPLICATIONS

BY

JAMES LOUIS EDUCATO

B.S., University of Notre Dame, 1985

THESIS

Submitted in partial fulfillment of the requirements
for the degree of Master of Science in Electrical Engineering
in the Graduate College of the
University of Illinois at Urbana-Champaign, 1988

Urbana, Illinois

ACKNOWLEDGEMENTS

I would like to thank Professor J. P. Leburton and the National Aeronautics and Space Administration for their support.

The many helpful discussions with Mike Wagner are gratefully acknowledged.

I would also like to acknowledge the support and encouragement of my parents, who motivated me to pursue graduate studies.

PRECEDING PAGE BLANK NOT FILMED

TABLE OF CONTENTS

Page

1. INTRODUCTION 1

2. DEVICE STRUCTURE AND CIRCUIT CONFIGURATION 4

3. MODELLING 9

4. RESULTS AND DISCUSSIONS 21

   4.1. AlGaAs-GaAs System 21

   4.2. AlGaAs-InGaAs System 25

5. CONCLUSIONS 35

   REFERENCES 36

1. INTRODUCTION

Solar cells convert spectral energy into electrical energy by a phenomenon known as the photovoltaic effect. Solar cells, also termed photovoltaics, are primarily used in space applications. Presently, solar cells provide power to more than five-hundred satellites. Photovoltaics are the logical choice for supplying power to space-based equipment because they provide nearly permanent, uninterrupted power and convert light directly into electricity without any intermediate stage. In addition, they possess a high power to weight ratio compared to other power sources [1]. For reasons of cost effectiveness and technological availability, the silicon (Si) pn junction design is currently the preferred choice for space-based power sources. But, the Si cell may not be the choice of the future. These cells have a relatively low beginning-of-life (BOL) efficiency of 15% [1]. Also, their performance is continuously degraded by exposure to the high energy particle environment of space which damages the semiconductor lattice, limiting the useful lifetime of the cell. Thus, there is an ongoing search for a photovoltaic design with higher BOL efficiency and better radiation tolerance. One of the most popular alternatives to Si cells are III-V cascade solar cell designs.

Cascade III-V photovoltaics have great potential. Many III-V compounds have direct energy gaps enabling them to absorb sunlight more effectively than Si which has an indirect energy gap. This allows thin-film III-V solar cells of lighter weight than thick-film Si cells. In addition, III-V lattices resist damage from radiation better than Si lattices. But most importantly, III-V's span a wide range of energy gaps and may be fabricated into monolithic, multijunction, multiband-gap structures known as cascade cells. Flexibility in selection of energy gap(s) for a solar cell

allows a more optimal use of available solar spectrum, and therefore, higher conversion efficiencies than for Si cells. Gallium arsenide (GaAs) single-gap cells have demonstrated efficiencies of 21% [2]. Cascade (multiband-gap) III-V photovoltaics have predicted efficiencies in excess of 30% [3]. The concept behind cascade cells is the division of the solar spectrum among two or more pn junction cells, known as subcells, each with different energy gaps. This concept may be illustrated with the operation of a two-gap cell.

The two-gap cascade cell is formed by epitaxially growing two subcells in a vertical stack with the higher-energy-gap subcell on top and the lower-energy-gap subcell on the bottom. The upper subcell absorbs sunlight with energy greater than its energy gap. The lower subcell absorbs radiation with energy less than the upper subcell gap and greater than the lower subcell gap. The cascade approach more optimally partitions the solar spectrum because the average difference between the initial energy of a photoexcited minority carrier and the energy gap of the subcell is smaller when there are two available energy gaps rather than one. Photogenerated minority carriers with energy above the energy gap relax to the band edge losing their excess energy to the lattice. In principle, higher conversion efficiency with cascade cells is possible than with single-gap cells by selecting the energy gaps of the two subcells to yield an optimal partition of the spectrum. Theoretically, even greater efficiency is possible with more than two energy gaps in a cascade structure because a finer partition of the solar spectrum may be obtained. However, the high cost and complexity of fabricating a two-gap monolithic III-V cascade cell have prevented the realization of the cascade cell's potential. To date, efficiencies of experimental cascade structures are lower than those of the best single-gap cells [4].

Currently proposed cascade cells have two problem areas that require special consideration: poor upper subcell performance and subcell interconnection. There is some concern that existing cascade designs will suffer appreciable performance degradation due to radiation damage to the upper subcell [5]. In addition, most proposed cascade designs are monolithic series cascade cells which require an intercell ohmic contact (IOC) imbedded between the two subcells. But, reliable fabrication of low loss, large area monolithic IOCs has proven difficult [6], particularly for lattice-mismatched systems like AlGaAs-InGaAs [7]. There is also concern that radiation induced degradation will cause substantial current mismatch losses in series cascade cells, resulting in low end-of-life (EOL) efficiencies [5].

As an alternative to existing silicon cells and currently proposed space-based photovoltaics, a novel class of three-terminal, multijunction, multiband-gap solar cells (MJSC) is presented [8]. MJSCs are three-terminal devices with multiple homojunctions in the upper subcell which improve the overall spectral response (and thus radiation tolerance) by decreasing the average distance carriers must diffuse before they are collected. Selective electrodes are used to achieve a three-terminal design which avoids the complications of fabricating a monolithically imbedded IOC between the two subcells and the joule losses associated with such a contact. Simulations of the MJSC design were performed for two material systems: AlGaAs-GaAs and AlGaAs-InGaAs. The AlGaAs-GaAs system is lattice-matched and has well-documented material parameters. On the other hand, the AlGaAs-InGaAs system is more interesting because it allows optimal partitioning of the solar spectrum.

2. DEVICE STRUCTURE AND CIRCUIT CONFIGURATION

Cross-sectional views of five- and seven-layer MJSC structures are shown in Figure 1a. The seven-layer MJSC has three homojunctions in its upper subcell, while the five-layer MJSC has just one. The five-layer MJSC design is similar to the three-terminal two-junction cascade cell fabricated in the lattice-matched AlGaAs-GaAs material system by Lewis et al. [7]. The principal difference between the two designs is in the contact to the base of the upper subcell and emitter of the lower subcell (note: both are of the same doping type). In the Varian cell, the "middle" contact to the heterojunction is made by etching a window in the upper subcell. AlGaAs-GaAs cascade cells fabricated with this design have shown one-sun, AM2 efficiencies of up to 21.0%. In the five-layer MJSC, the "middle" contact is a heavily doped region known as a selective electrode (the n^+ region in Figure 1a).

The seven-layer MJSC with additional homojunctions in the upper subcell has shown potential for improvement over the five-layer MJSC and other similar cascade designs, such as the one made by Lewis et al. Additional homojunctions in the upper subcell enhance spectral response (the fraction of photoexcited carriers that contribute to short-circuit current) and improve radiation tolerance. The collection probability for minority carriers is essentially determined by the semiconductor minority-carrier diffusion length and the distance to a homojunction. Multiple homojunctions reduce the average distance from photogenerated carriers to the nearest junction (Figure 1b). By reducing the average distance photoexcited minority carriers must diffuse before encountering a junction, the probability of carriers being collected before they recombine is increased. Since radiation damage to the semiconductor lattice degrades the minority-carrier diffusion lengths, the additional

a)

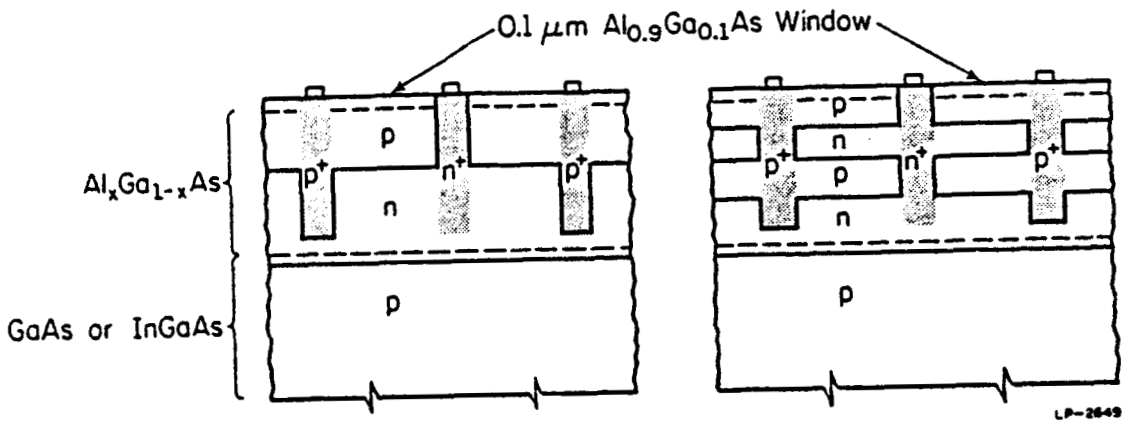

b)

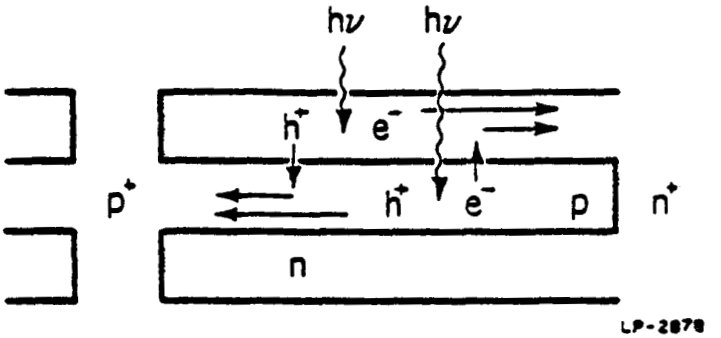

Figure 1. Conceptual diagram of five- and seven-layer MJSC structures showing a) schematic cross-sectional views and b) details of carrier collection and lateral transport to selective electrodes. Isotype heterojunctions and homojunctions are represented by dashed lines and solid lines, respectively. The third contact to the substrate is not shown.

homojunctions also upgrade radiation tolerance. The use of multiple homojunctions represents the only available means for improving spectral response given fixed material parameters. However, a trade-off exists between spectral response improvement and increased dark current from the additional junctions. Typically, three junctions are optimal for the upper cell.

Multiple junctions in the MJSC upper subcells preclude transport of collected carriers in the direction transverse to the layers. Instead, collected carriers are transported in the layer planes to heavily doped regions extending vertically through the superstructure (Figure 1b). These heavily doped regions are known as selective electrodes since they connect only to layers of like doping. Junctions with layers of opposite doping type are reverse-biased during normal operation. Any number of additional junctions can be incorporated into the upper subcell with this technique. Selective electrodes have been used in other multilayer devices, such as an avalanche photodiode suggested by Capasso [9]. Recently, an ingenious method of growing selective electrodes for NIPI doping superlattices has been proposed by Dohler [10]. This method allows in situ fabrication of selective electrodes for higher doping concentrations than was previously possible.

As mentioned in the introduction, MJSCs use selective electrodes to achieve a three-terminal design. Although the commercial viability of three-terminal photovoltaics has been discounted by many researchers [7,11], problems with array interconnection of three-terminal devices can be solved by creating two-terminal units from complementary pairs [12] (npn and pnp) of three-terminal cells as shown in Figure 2. The upper subcell current of one three-terminal cell must be matched to the lower subcell current of the complementary three-terminal cell. Such two-

a)

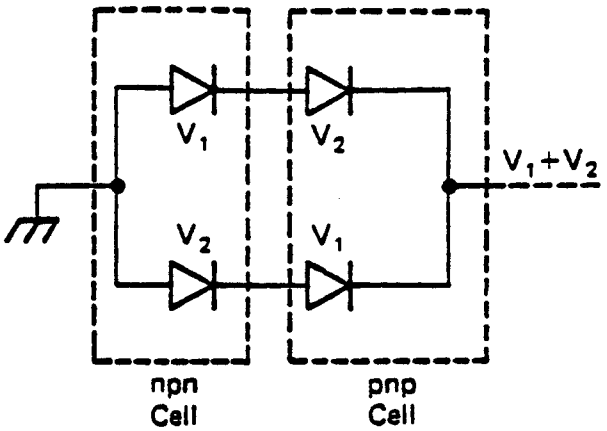

b)

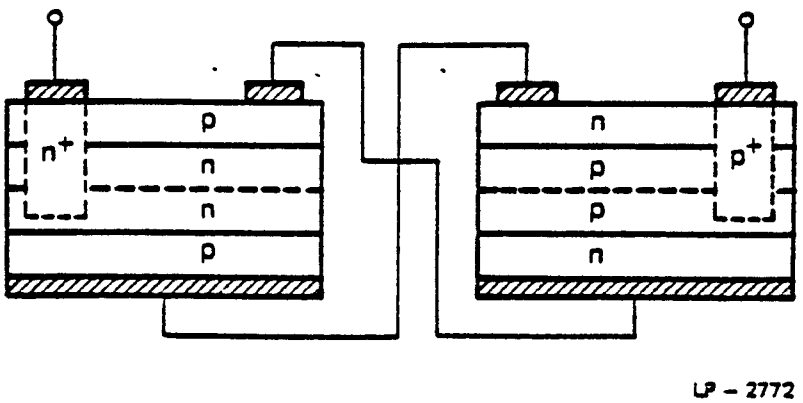

Figure 2. Complementary interconnection scheme for three-terminal photovoltaics showing a) electrical configuration and b) one possible physical configuration.

terminal pairs may then be incorporated into practical arrays. A promising connection scheme has recently been proposed by Gee [13], which avoids the need for a complementary cell by using by using a 1 x 2 voltage-matched configuration.

3. MODELLING

In order to model cascade solar cells, principles of single-bandgap solar cell operation must be understood. Shown in Figure 3 are energy band diagrams of illuminated pn junction solar cells, both short-circuited and under load. Incident photons with energy greater than that for the bandgap are absorbed by the semiconductor, creating electron-hole pairs. If the excess minority carriers diffuse to the edges of the space-charge region without recombining, the strong built-in field of the space-change region will sweep carriers across the junction, giving rise to a photocurrent, and therefore, a photovoltage across the load. The polarity of the output voltage is the same as the forward-bias direction of the cell (pn junction) because the current delivered to the load is in the direction opposite the forward-bias current through the nonilluminated cell. If the cell's terminals are short-circuited, there will be no bias across the junction and, consequently, the entire photocurrent will flow. When the cell drives a load, the pn junction is forward-biased giving rise to another component of current known as dark current. Thus, the fundamental circuit model is a current source shunted by a diode (Figure 4). The current source represents the photocurrent collected across a junction and the diode represents dark current shunted away from the output by the junction. This model assumes the superposition of photocurrent and dark current. This assumption is not valid under the high-injection conditions ($p \approx n$ in quasi-neutral regions) of high solar concentration.

The most commonly used electrical characteristics of a cell are short-circuit-current density, open-circuit voltage, fill factor, and efficiency. The fill factor is the ratio of maximum cell output power to the product of short-circuit current and

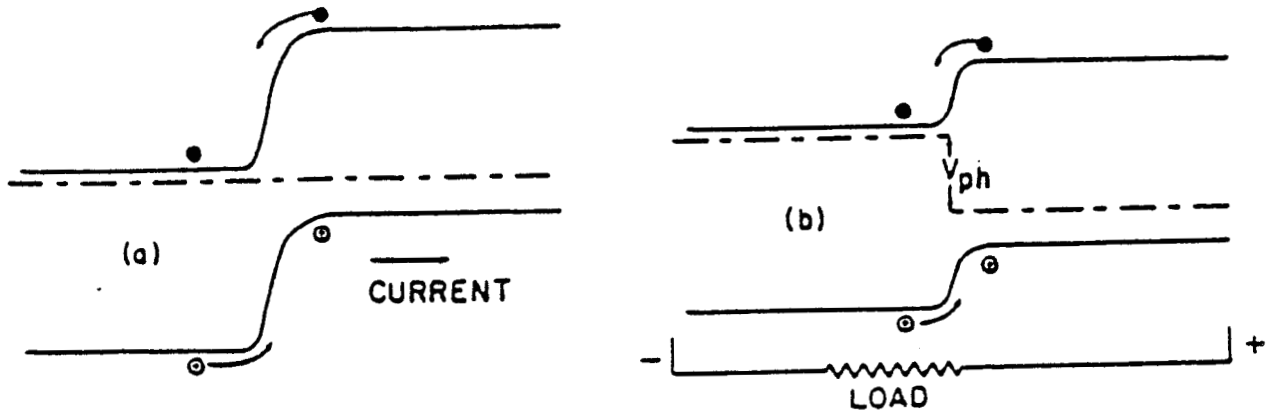

Figure 3. Energy band diagram of an illuminated pn junction solar cell : a) short-circuited; b) under load.

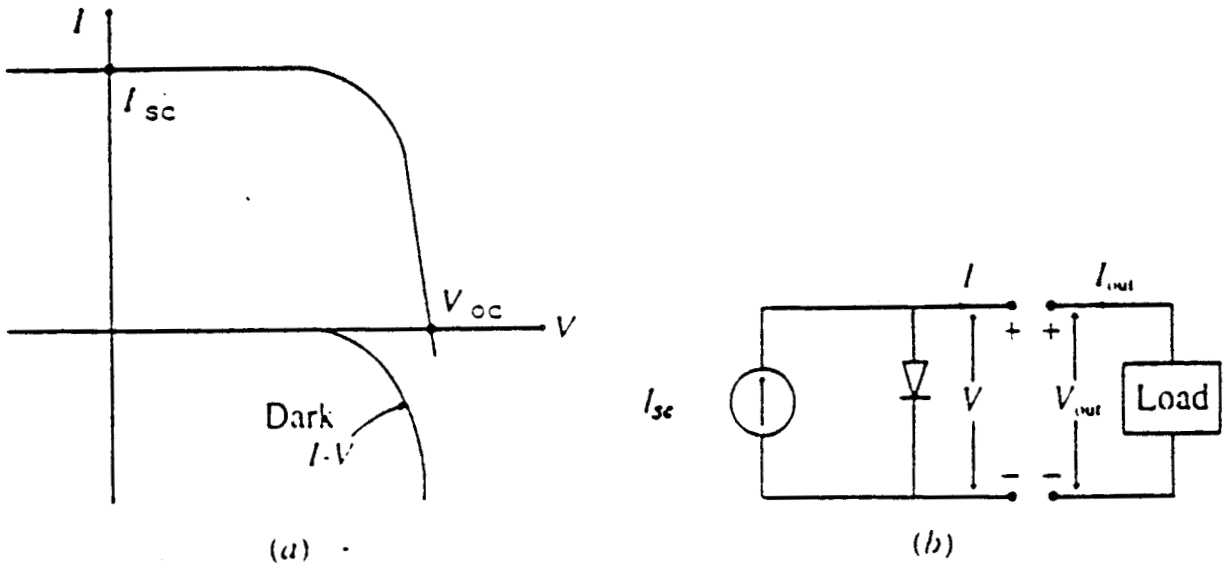

Figure 4. a) Superposition of short-circuit current and dark current yields the I-V curve of a solar cell. b) Cell I-V curve and load determine the output current and voltage.

open-circuit voltage. The efficiency is the ratio of cell output power to incident solar power.

With some of the basic principles already discussed, the operation of single-bandgap photovoltaics will be examined in more detail. At the top of the structure is a thin layer of high-energy-gap material (usually AlGaAs), known as a window layer, which allows almost all of the solar spectrum to pass through it without being absorbed. The surface of the window layer usually has an antireflection (AR) coating. The window provides an interface to the uppermost active layer of the cell, known as the emitter, with a much lower recombination velocity than would occur at a surface. Note that even though there are materials with different energy gaps within the cell, this structure is not a cascade cell. Recall, the cascade cell design calls for two or more subcells (each subcell contains at least one pn junction) made out of materials with different energy gaps. Below the window layer are the active layers which form the pn junction(s). A buffer layer electrically connects the last active layer and the substrate.

The dark current is comprised of injection and space-charge recombination components. The injection component is due to the unbalanced diffusion currents caused by the lowering of the junction potential when forward bias is applied. This component may be modelled by the Shockley diode equation. Generally, the boundary conditions used for the minority carrier concentrations at the quasi-neutral region edges away from the junction incorporate surface recombination velocities. In this way, different geometries may be easily handled. For example, a pn junction bounded by a heterojunction or buffer layer may be modelled with the same expression by changing only the value of surface recombination velocity used. The expres-

sion for injection current derived in this manner may be easily found [1]. The space-charge recombination component results from the carrier recombination that occurs within the depletion region. This may be modelled by adding a term to the Shockley diode equation. Space-charge recombination will always dominate the injection component in a cell made in the AlGaAs alloy system operated at its maximum-power point [14].

Short-circuit current is found by dividing the solar spectrum into many segments, each having a narrow range of wavelength, and finding the current due to each spectral segment. Each spectral segment is assigned a single wavelength and absorption coefficient allowing the carrier generation rate to be expressed as a function of distance. Thus, short-circuit current is found by calculating the contributions of all regions for the solar flux at a given wavelength, starting at the top of the structure and working down, taking into account the reduction in photon flux as the light passes through each region. The total short-circuit current is the sum over regions which contribute at a given wavelength and over the relevant range of wavelengths. Spectral superposition is valid since the differential equations and boundary conditions governing the photoexcited minority-carrier populations are linear. These expressions may be found by solving the minority-carrier continuity equations with the appropriate boundary conditions. The boundary condition of zero excess minority-carrier concentration at the depletion-region edges and the incorporation of surface recombination velocities into the boundary condition for edges of the neutral region away from the junction yield an expression for short-circuit current which may be used for most cell geometries [1]. In addition to the quasi-neutral regions, window layer and depletion-region contributions to short-

circuit current must be considered. An expression for the window-layer contribution may be found in reference [15]. The contribution from the depletion region may be easily found by assuming 100% collection of carriers photogenerated in the depletion region [1]. This assumption is reasonable since the large space-charge field will rapidly sweep minority carriers across the junction.

To complete the single-bandgap, single homojunction model, resistive losses should be considered. There are two types of resistance: shunt and series. Shunt resistance can be caused by surface leakage along the edges of the cell, by diffusion spikes along dislocations or grain boundaries, or possibly by fine metallic bridges along microcracks, grain boundaries, or crystal defects such as stacking faults after the contact metallization has been applied [1]. Shunt resistance effects are important at very low levels of illumination. Series resistance can arise from contact and layer resistance. Series resistance effects are important under high solar concentration. Since neither very low nor very high levels of illumination are considered (operation under one-sun AMO conditions is assumed), shunt and series resistances are neglected in all simulations.

The modelling of solar cells with multiple homojunctions (as in the upper subcell of MJSCs) will now be addressed. If shunt and series resistances are included, the modelling of these structures is considerably more complicated than for the single homojunction solar cell. But with resistive losses neglected, the multiple homojunction cell or subcell may be modelled as a composite current source shunted by multiple diodes. The composite current source is the sum of the short-circuit current contributions of each layer, and the multiple diodes represent the loading effects of the junctions.

Individual subcells of a cascade photovoltaic may be modelled as single-gap cells. With each subcell modelled, the only issue left to consider is how the subcells are electrically interconnected. There are two cases to be considered: a two-terminal configuration and a three-terminal configuration. The performance potential of the two- and three-terminal cascade cells was evaluated by means of a detailed computer model which allows a wide variety of multilayer, multiband-gap structures to be investigated. Effects of the selective electrode regions on the minority-carrier distribution are assumed to be negligible, permitting a one-dimensional analysis. Since both p- and n-type electrodes are necessary, an interdigitated front-surface grid array is required. Grid obscuration is assumed to be 4%, attainable with existing grid array technology [2]. A 300 angstrom $Al_{0.9}GA_{0.1}As$ window with Si_3N_4 antireflection coating [16] and surface recombination velocity of 10^6 cm/s is assumed. The absorption coefficient is modelled as in reference [17]. Doping and composition profiles are assumed to be uniform within each layer and abrupt at junctions.

These assumptions allow closed-form expressions to be used for the contributions of each layer to short-circuit current, injection current, and space-charge recombination. Each design was optimized with respect to layer thickness and composition via a constrained optimization technique extended from Rosenbrock's algorithm [18, 19]. This method of optimization combines generalized constrained optimization techniques and device modelling techniques into an optimization cycle that automatically adjusts the values of all structure parameters at the same time under several constraints until the requirements are satisfied. In many other modelling approaches, cells are optimized with respect to only some structure parameters

with the others fixed. By neglecting the interaction between parameters, the resulting design may not be optimal. In this new method of solar cell optimization, all parameters to be optimized are simultaneously adjusted in a systematic manner, resulting in a truly optimum design. The optimization criterion used was to maximize beginning-of-life (BOL) efficiency with the subcells operating at their individual maximum-power points. This criterion does not yield an estimate of cell performance in a complementary configuration, which will require the pnp and npn cells to be simultaneously optimized because of the current-matching requirement already discussed. However, simulations of two-terminal MJSC structures with ideal IOCs very closely approximate the performance of the complementary configuration. For this reason, two-terminal MJSC structures are modeled with electrically and optically lossless IOCs.

The current-voltage (I-V) characteristics of the three-terminal MJSCs are represented by an Ebers-Moll model. The coupled-diode equations are

$$J_1(v_1,v_2) = J_{sc_1} - J_{o_{11}} e^{\lambda v_1} - J_{o_{12}} e^{\lambda v_2} - \sum_{m=1}^{N_1} J_{gr_m}^{(1)} \left\{ \frac{e^{\lambda v_1/2}}{v_{b_m} - v_1} \right\} \tag{1.a}$$

$$J_2(v_1,v_2) = J_{sc_2} - J_{o_{21}} e^{\lambda v_2} - J_{o_{22}} e^{\lambda v_1} - \sum_{m=1}^{N_2} J_{gr_m}^{(2)} \left\{ \frac{e^{\lambda v_2/2}}{v_{b_m} - v_2} \right\} \tag{1.b}$$

where $\lambda = q/kT$ and the subscript one refers to the upper subcell. The terms J_{sc_1} and J_{sc_2} represent the upper and lower subcell short-circuit current densities, respectively. Coefficients $J_{o_{11}}$, $J_{o_{12}}$, $J_{o_{21}}$, and $J_{o_{22}}$ determine the dependence of the injected component of the dark current on the subcell terminal voltages. (Note: $J_{o_{12}}$ and $J_{o_{21}}$ are zero for the two-terminal configuration since the minority-carrier populations cannot interact across the IOC separating the subcells.) For conciseness, the sums over individual layer contributions to short-circuit and injection components of

dark current are not explicitly written out; rather, the J_{sc_1}, J_{sc_2}, $J_{o_{11}}$, and $J_{o_{22}}$ coefficients are composite values. This is not the case for $J_{o_{12}}$ and $J_{o_{21}}$ since only one layer of the adjacent subcell contributes to the coupled injection component of dark current. Coupling of the I-V equations arises from interaction of the injected minority-carrier concentrations across the heterojunction separating the upper and lower subcells.

The remaining terms represent the space-charge recombination component of the dark current. Each summation is over the homojunctions contained in the corresponding subcell. It is necessary to have a term for each junction because the barrier potentials (v_{b_m}'s) will not be the same for all junctions in a particular subcell. If they were identical, the voltage-dependent terms would factor out and one could simply sum over the J_{gr_m}'s to obtain a composite coefficient as in the case of the short-circuit and injected current terms. The J_{gr_m}'s were calculated using Choo's theory of space-charge recombination for abrupt, asymmetrical junctions [20]:

$$J_{gr_m} = \frac{\pi n_i W k_B T}{2} \sqrt{\tau_{po} \tau_{no}} \tag{2}$$

where n_i is the intrinsic carrier concentration; W is the depletion width; τ_{po} and τ_{no} are the lifetimes in the depleted region.

Expressions for contributions of the window, emitter (upper subcell), and base (lower subcell) to the short-circuit and injected currents are well-known and have been published elsewhere [1, 15]. Contributions of layers bounded above and below by homojunctions are easily derived from the minority-carrier continuity and current-density equations with the boundary condition of zero excess carrier density at the depletion-region edges:

$$J_o^k = \frac{2qD_n n_i^2}{L_n N_A}\left[\frac{\cosh[(t_k'/L_n) - 1]}{\sinh(t_k'/L_n)}\right] \tag{3}$$

$$J_{sc}^k(\lambda) = \frac{qF_k\alpha L_n}{\alpha^2 L_n^2 - 1}\left\{\alpha L_n(1-e^{-\alpha t'_k}) - (1+e^{-\alpha t'_k})\left[\frac{\cosh[(t'_k/L_n) - 1]}{\sinh(t'_k/L_n)}\right]\right\} \tag{4}$$

where t'_k is the thickness of the kth layer quasi-neutral region; N_A. L_n. and D_n are the donor concentration, electron diffusion length, and diffusion coefficient, respectively, for a p-doped layer (the corresponding quantities for an n-doped layer are N_D, L_p, and D_p); and q is the charge of an electron. The quantity α is the absorption coefficient, and F_k is the photon flux incident on the quasi-neutral region of the kth layer. Both depend on the wavelength (λ) of the incident radiation. A summation over the incident solar spectrum must therefore be performed. Data for the AMO solar spectrum were taken from reference [21].

The contributions of layers adjacent to the isotype heterojunction that separates the upper and lower subcells are considerably more complicated to calculate because interaction between minority-carrier populations in the layers above and below the heterojunction must be taken into account. The barrier seen by minority carriers at the heterojunction is the junction built-in potential. Doping concentrations in the adjacent layers are sufficiently high that the heterojunction bias will be effectively zero for typical current densities. For a p-doped junction, the boundary conditions on the minority-carrier concentrations are

$$n_{p_1}/n_{p_2} = \exp[(E_{F_1} - \Delta E_G - E_{F_2})/k_B T] \tag{5.a}$$

$$D_{n_2}\nabla n_{p_2} = S_n \Delta n_{p_2} + D_{n_1}\nabla n_{p_1} \tag{5.b}$$

The Fermi levels E_{F_1} and E_{F_2} are measured from the respective valence band edges. Subscript one denotes the upper subcell. S_n is the interface recombination velocity

at the heterojunction. These boundary conditions are nearly identical in form to those described for low-high junctions [22]. The only differences are the ΔE_G term, which must be included in the expression for the junction barrier potential because of the band edge discontinuity at the heterojunction, and a term to account for recombination at the heterostructure interface. Using these boundary conditions, the contributions to the injection component of dark current of layers adjacent to a p-doped isotype heterojunction are

$$J_{0_{11}} = \frac{qD_{n_1}n_{i_1}^2}{L_{n_1}N_{A_1}} \left[\frac{S_1S_2D_{n_1}L_{n_2}\exp(-qV_{mj}/k_BT) + C_1L_{n_1}(S_2L_{n_2}S_n + D_{n_2}C_2)}{C_1S_2D_{n_1}L_{n_2}\exp(-qV_{mj}/k_BT) + S_1L_{n_1}(S_2L_{n_2}S_n + D_{n_2}C_2)} \right] \tag{6.a}$$

$$J_{0_{12}} = \frac{qD_{n_1}n_{i_2}^2}{L_{n_1}N_{A_2}} \left[\frac{-D_{n_2}L_{n_1}\exp(-qV_{mj}/k_BT)}{C_1S_2D_{n_1}L_{n_2}\exp(-qV_{mj}/k_BT) + S_1L_{n_1}(S_2L_{n_2}S_n + D_{n_2}C_2)} \right] \tag{6.b}$$

$$J_{0_{21}} = \frac{qD_{n_1}n_{i_1}^2}{L_{n_1}N_{A_1}} \left[\left(\frac{D_{n_2}}{D_{n_2}C_2 + S_2L_{n_2}S_n} \right) \times \right.$$

$$\left. \left(S_1 - C_1 \frac{S_1S_2D_{n_1}L_{n_2}\exp(-qV_{mj}/k_BT)+C_1L_{n_1}(D_{n_2}C_2+S_2L_{n_2}S_n)}{C_1S_2D_{n_1}L_{n_2}\exp(-qV_{mj}/k_BT)+S_1L_{n_1}(D_{n_2}C_2+S_2L_{n_2}S_n)} \right) \right] \tag{6.c}$$

$$J_{0_{22}} = \frac{qD_{n_2}n_{i_2}^2}{L_{n_2}N_{A_2}} \left[\left(\frac{L_{n_2}}{D_{n_2}C_2+S_2L_{n_2}S_n} \right) \left(\frac{D_{n_1}D_{n_2}C_1\exp(-qV_{mj}/k_BT)}{C_1S_2D_{n_1}L_{n_2}\exp(-qV_{mj}/k_BT)+S_1L_{n_1}(D_{n_2}C_2+S_2L_{n_2}S_n)} \right.\right.$$

$$\left.\left. + \frac{S_2D_{n_2}+C_2L_{n_2}S_n}{L_{n_2}} \right) \right] \tag{6.d}$$

where S_1 is the hyperbolic sine of the ratio of the thickness of the quasi-neutral region in the larger energy-gap material (upper subcell) to the minority diffusion length, and S_2 is the hyperbolic sine of the ratio of the thickness of the quasi-neutral

region in the smaller energy-gap material (lower subcell) to the minority diffusion length. Likewise, C_1 and C_2 represent ratios involving hyperbolic cosines, and $qV_{mj}=\Delta E_G+E_{F_2}-E_{F_1}$. The contributions of these layers to short-circuit current are

$$J_{sc_1} = \frac{D_{n_1}B_1}{L_{n_1}} + \alpha_1 L_{n_1} F_1 Q_1 \tag{7.a}$$

$$J_{sc_2} = -\frac{D_{n_2}}{L_{n_2}}(AS_2+B_2C_2) - \alpha_2 L_{n_2} Q_2 F_1 E_1 E_2 \tag{7.b}$$

where

$$A = \frac{F_1 Q_2 E_1 E_2 L_{n_2}}{D_{n_2} C_2} - \frac{S_2 B_2}{C_2} \; : \tag{8.a}$$

$$B_1 = F_1 \left[\frac{\frac{Q_1 L_{n_1}^2}{D_{n_1}}(E_1-C_1)(S_2L_{n_2}S_n+D_{n_2}C_2) - Q_1S_2L_{n_1}L_{n_2}(S_1+\alpha_1L_{n_1}E_1)\exp(-qV_{mj}/k_BT)}{C_1S_2D_{n_1}L_{n_2}\exp(-qV_{mj}/k_BT)+S_1L_{n_1}(S_2L_{n_2}S_n+D_{n_2}C_2)} \right.$$

$$\left. - \frac{Q_2E_1L_{n_1}L_{n_2}(C_2-E_2-\alpha_2L_{n_2}S_2)\exp(-qV_{mj}/k_BT)}{C_1S_2D_{n_1}L_{n_2}\exp(-qV_{mj}/k_BT)+S_1L_{n_1}(S_2L_{n_2}S_n+D_{n_2}C_2)} \right] \tag{8.b}$$

$$B_2 = \frac{F_1\{S_nQ_2L_{n_2}^2E_1(E_2-C_2)/D_{n_2} - L_{n_2}C_2[\alpha_2L_{n_2}Q_2E_1 - Q_1(S_1+\alpha_1L_{n_1}E_1)]\} + B_1C_1C_2L_{n_2}D_{n_1}/L_{n_1}}{S_2L_{n_2}S_n+D_{n_2}C_2} \tag{8.c}$$

$$Q_1 = \frac{\alpha_1 L_{n_1}}{\alpha_1^2 L_{n_1}^2 - 1}; \tag{8.d}$$

$$Q_2 = \frac{\alpha_2 L_{n_2}}{\alpha_2^2 L_{n_2}^2 - 1}; \tag{8.e}$$

$$E_1 = \exp(-\alpha_1 t'_1); \tag{8.f}$$

$$E_2 = \exp(-\alpha_2 t'_2); \tag{8.g}$$

F_1 is the flux incident upon the top of the isotype heterojunction; α_1 and α_2 are the absorption coefficients in the upper and lower subcells, respectively; and t'_1 and t'_2 are the thicknesses of the quasi-neutral regions adjacent to the isotype heterojunction.

4. RESULTS AND DISCUSSION

4.1. AlGaAs-GaAs System

For simulations of AlGaAs-GaAs MJSCs, mobilities and diffusion lengths are computed as functions of doping concentration and alloy composition, using empirical relations for the dependence on doping in GaAs [23]. These were modified for AlGaAs by including a polar-optical-phonon scattering term to account for the effect of alloy composition [24]. Simulations of AlGaAs-GaAs MJSCs were performed for the five- and seven-layer three-terminal structures shown in Figure 1. Since these simulations are for the three-terminal MJSCs with each subcell operating at its maximum power point, the following results will not be expected for the complementary configuration.

We found that efficiencies of optimized five- and seven-layer three-terminal AlGaAs-GaAs MJSCs vary gradually with upper subcell composition and have broad peaks at AlAs mole fraction x=0.36, which corresponds to an energy gap of 1.87 eV (Figure 5). The seven-layer MJSC has upper subcell layer widths ranging from 0.1 μm to 3 μm. Both structures are predicted to have maximum BOL one-sun AMO efficiencies in excess of 28% without space-charge recombination effects and in excess of 26% with space-charge recombination taken into account. The data neglecting space-charge recombination are included for purposes of comparison with other groups [25]. A detailed discussion of the effects of space-charge recombination as a function of the AlAs mole fraction in the upper subcell has been reported in a previous publication [8].

The spectral response of a five-layer MJSC with optimum upper subcell composition (x=0.36) is shown in Figure 6. Curves for the individual layer contributions

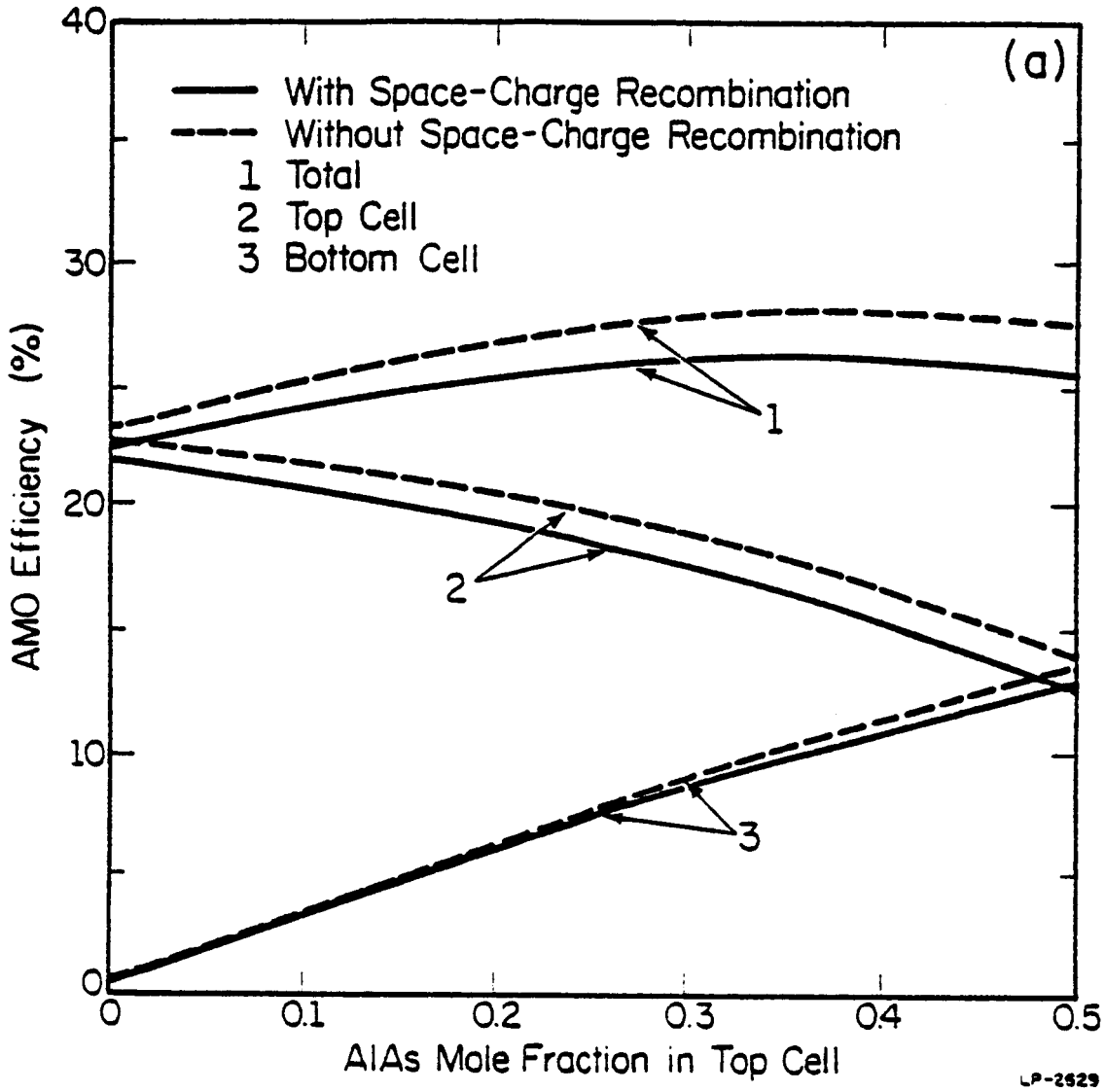

Figure 5. Performance of AlGaAs-GaAs MJSCs under one-sun AMO illumination (300 K): a) five-layer structure;

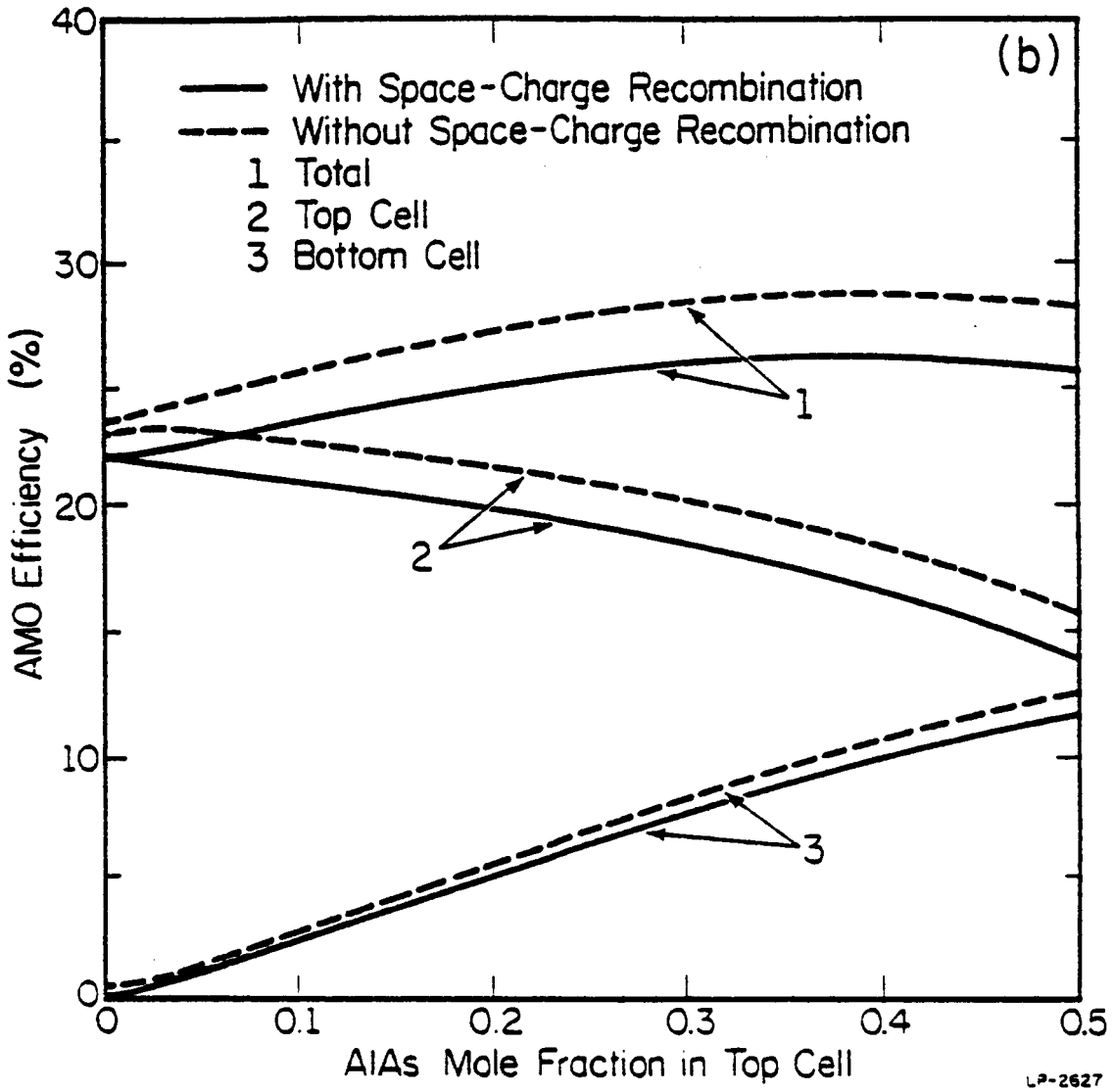

Figure 5. contd. b) seven-layer structure.

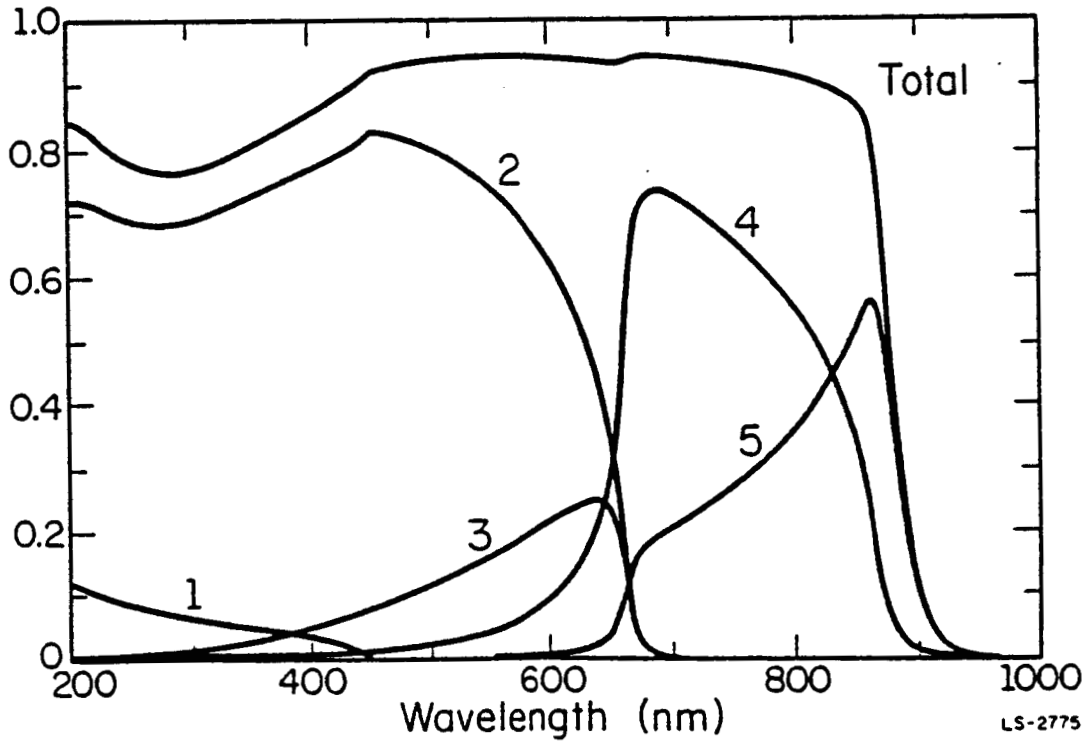

Figure 6. Spectral response of a five-layer AlGaAs-GaAs MJSC with upper subcell composition x = 0.36. Individual layer contributions are shown (numbered) as well as total spectral response. Layers one, two, and three are the window, emitter, and base, of the upper subcell; layers four and five are the emitter and base of the lower subcell.

include both depletion and quasi-neutral region responses. The overall response (upper curve) of the five-layer MJSC is seen to be greater than 0.8 for most wavelengths. The overall spectral response curve for the seven-layer MJSC (not shown) has a sharper knee at wavelengths near the bandgap of AlGaAs, since deeper junctions collect carriers photoexcited by lower-energy photons.

Although the predicted BOL efficiencies of the five-and seven-layer AlGaAs MJSCs are nearly identical, the effect of the two additional homojunctions in the upper subcell of the seven-layer design becomes noticeable when the cell's performance is degraded after exposure to radiation. The performance of the three-terminal AlGaAs-GaAs MJSCs as diffusion lengths within each cell are uniformly degraded is shown in Figure 7. As damage to the lattice from radiation accumulates, the performance of the seven-layer MJSC improves relative to that of the five-layer MJSC. Assuming an end-of-life (EOL) efficiency of 75% of BOL efficiency and uniform deterioration of diffusion lengths with time, we can estimate that the seven-layer MJSC will operate about 22% longer than the five-layer MJSC.

4.2. AlGaAs-InGaAs System

Since information on InGaAs minority-carrier diffusion lengths is sparse, simulations of AlGaAs-InGaAs MJSCs [26] were performed for plausible values (ranging from 1 to 6 μm) of InGaAs electron diffusion lengths. A fixed value of 2 μm was assumed for the hole diffusion length. Maximum BOL one-sun AMO conversion efficiency versus InGaAs electron diffusion length for the two MJSC structures is shown in Figure 8. These results are for the three-terminal MJSCs with each subcell operating at its maximum power point. With space-charge recombination effects included, the model predicts BOL efficiencies for the seven-layer MJSC in excess of

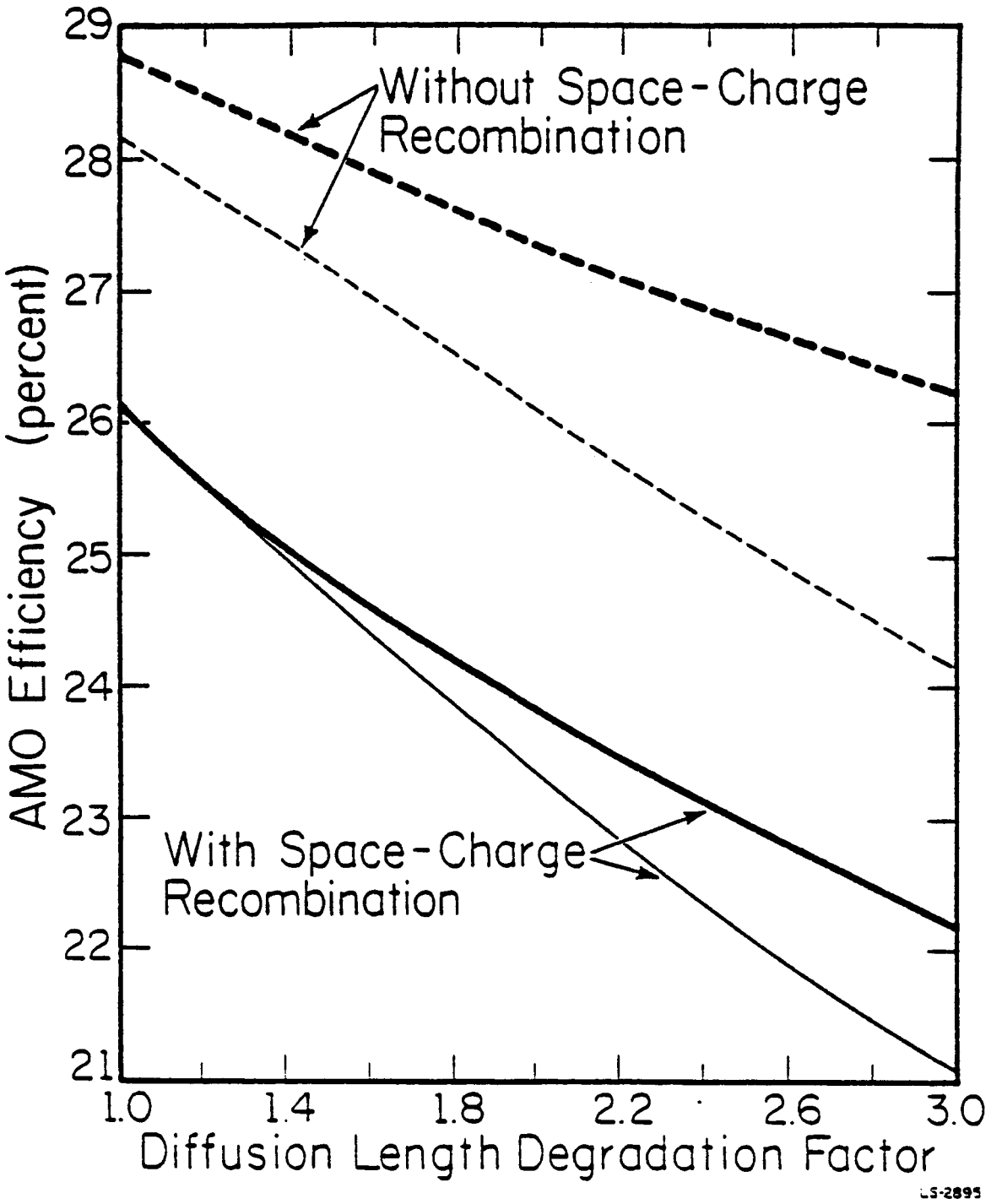

Figure 7. Effects of radiation damage on seven-layer (thick lines) and five-layer (thin lines) three-terminal AlGaAs-GaAs MJSCs. Progressive lattice damage is simulated by decreasing diffusion lengths.

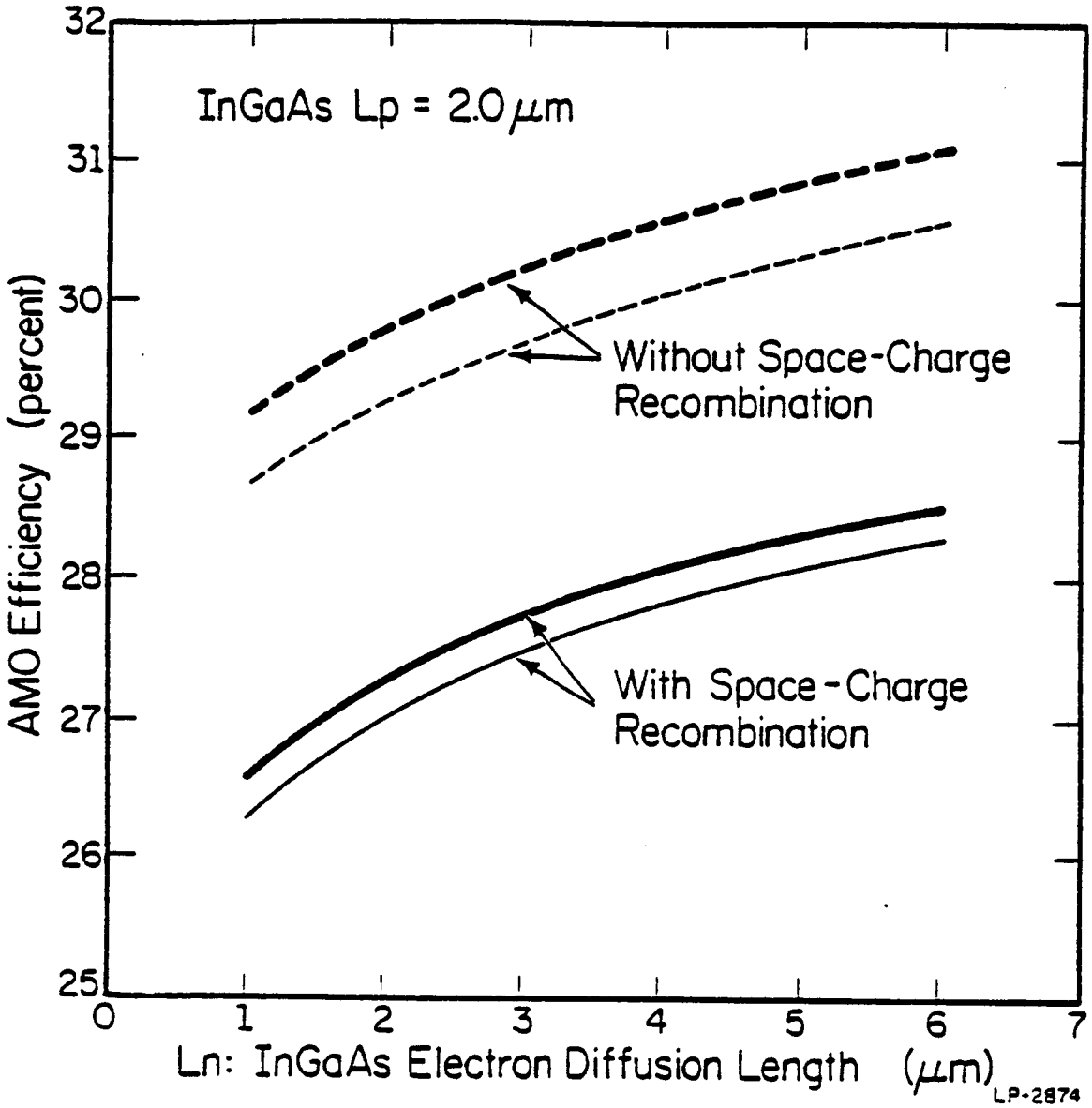

Figure 8. Beginning-of-life efficiencies of the seven-layer (thick lines) and five-layer (thin lines) three-terminal AlGaAs-InGaAs MJSCs versus InGaAs electron diffusion length under one-sun AMO illumination (L_p = 2.0 μm, T = 300 K). The dashed curves represent efficiencies that would be obtained if space-charge recombination were suppressed.

28% for InGaAs $L_n \geqslant 3.7\ \mu m$. The efficiencies of both optimized MJSC structures vary gradually with subcell composition. Both MJSCs have an optimum upper subcell energy gap of 1.6 eV, which corresponds to a composition of about x=0.2 (AlAs mole fraction). The optimum lower subcell energy gap was found to be roughly 1.0 eV (InAs mole fraction of 0.4) for InGaAs $Ln \geqslant 3.0\ \mu m$. The additional junctions in the upper subcell improve the overall performance of the cell as seen by the slightly better BOL efficiencies of the seven-layer MJSC than that for the five-layer MJSC. The seven-layer MJSC has upper subcell layer widths ranging from 0.1 μm to 4 μm. The spectral response of an optimized five-layer MJSC is shown in Figure 9. As expected from the better material combination, the spectral response is improved with respect to the AlGaAs-GaAs system. Again, the seven-layer MJSC shows even better behavior at wavelengths near the bandgap of AlGaAs.

The additional homojunctions in the upper subcell of the seven-layer AlGaAs-InGaAs MJSC yield only a slight increase in BOL efficiency over the five-layer AlGaAs-InGaAs MJSC. The improvement becomes more pronounced as diffusion lengths are degraded. The performances of the three-terminal MJSCs as diffusion lengths within each cell are uniformly degraded are shown in Figure 10. The BOL InGaAs diffusion lengths are assumed to be 6.0 μm for electrons and 2.0 μm for holes. As damage to the lattice from radiation accumulates, the performance of the seven-layer MJSC (two additional homojunctions in the upper subcell) continues to improve relative to that of the five-layer MJSC. The seven-layer MJSC will therefore operate longer than the five-layer MJSC. With the same assumptions as for the AlGaAs-GaAs MJSCs, the lifetime of the seven-layer MJSC will be about 20% longer than that for the five-layer MJSC.

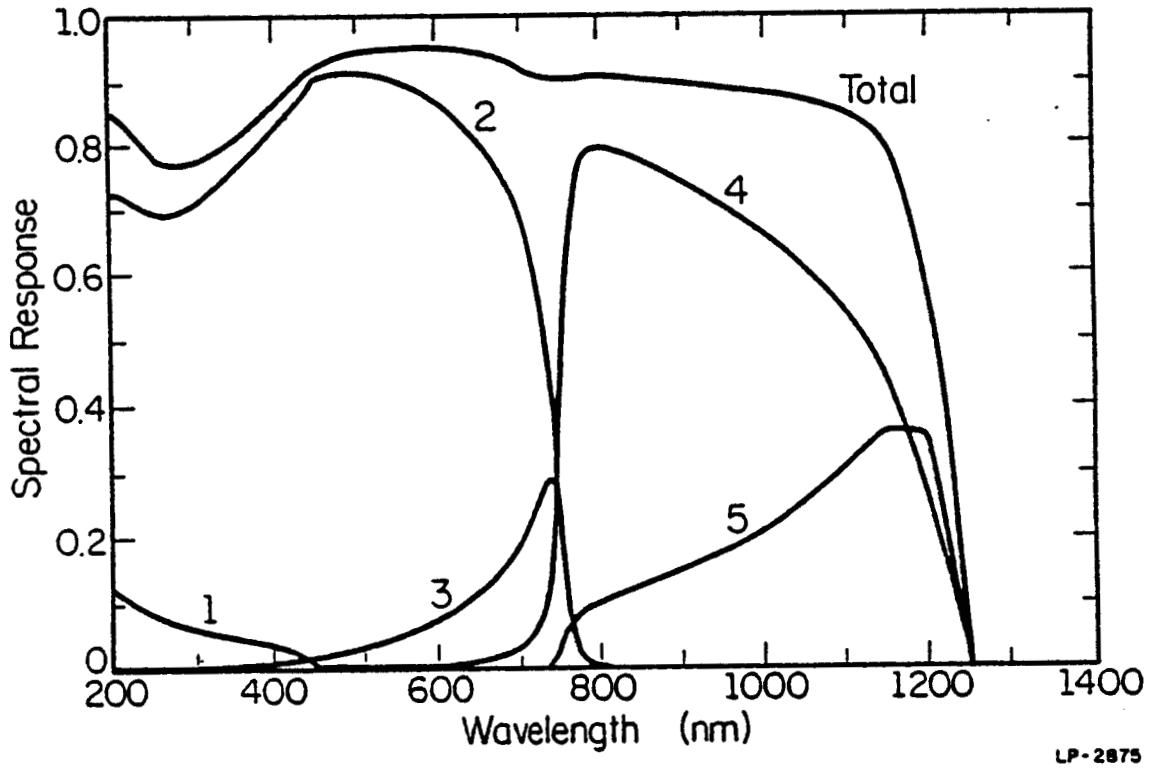

Figure 9. Spectral response of a five-layer AlGaAs-InGaAs MJSC showing individual layer contributions (numbered) as well as overall spectral response (uppermost curve). Curves for the individual layer contributions include both depletion and quasi-neutral region response.

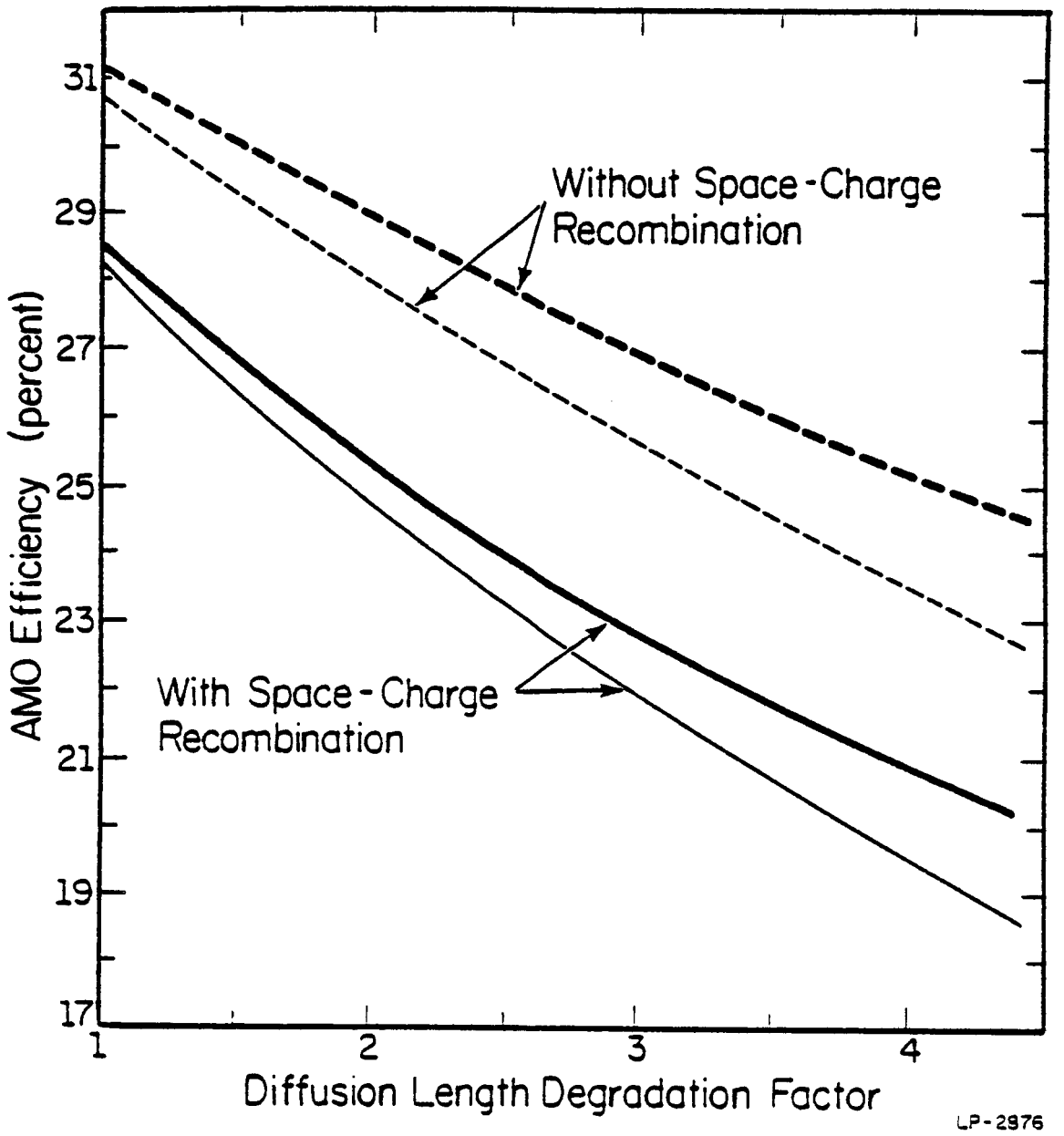

Figure 10. Effects of radiation damage on seven-layer (thick lines) and five-layer (thin lines) three-terminal AlGaAs-InGaAs MJSCs.

The efficiency of a complementary pair is expected to be very close to that of a two-terminal MJSC with an ideal IOC. The maximum BOL efficiency versus InGaAs electron diffusion length is shown in Figure 11 for two series-connected MJSC devices: a five-layer (n-np-np) structure and a six-layer (p-pnp-np) structure, both assumed to have ideal IOCs. The six-layer MJSC has BOL efficiency in excess of 27% (InGaAs $L_n \geqslant 2.5\ \mu m$) with space-charge recombination included. The six-layer MJSC with one additional homojunction in the upper subcell outperforms the five-layer MJSC with no additional homojunctions. The six-layer MJSC has upper subcell layer widths ranging from 0.4 μm to 4 μm. The six-and-five-layer MJSCs have optimum upper subcell energy gaps of about 1.7 eV and 1.75 eV, respectively, (AlAs mole fractions of 0.21 and 0.27, respectively) and lower subcell energy gaps of about 1.0 eV and 1.1 eV, respectively, (InAs mole fractions of 0.41 and 0.29, respectively).

The performances of five- and six-layer two-terminal MJSCs as diffusion lengths are degraded are shown in Figure 12. The BOL InGaAs diffusion lengths are the same as for the cells in Figure 10. Ideal IOCs are assumed in order to approximate the performance of the complementary configuration, which is composed of pairs of three-terminal cells having no IOCs that can degrade as would occur for a series cascade cell with a monolithically imbedded IOC. In all simulations, the IOCs of the series-connected (two-terminal) cells are therefore assumed to remain ideal even as layer diffusion lengths are degraded. Complementary pairs of multilayer MJSCs should decisively outperform cascade cells with monolithic IOCs. As damage to the lattice from radiation accumulates, the performance of the six-layer MJSC continues to improve relative to that of the five-layer MJSC. Assuming an EOL

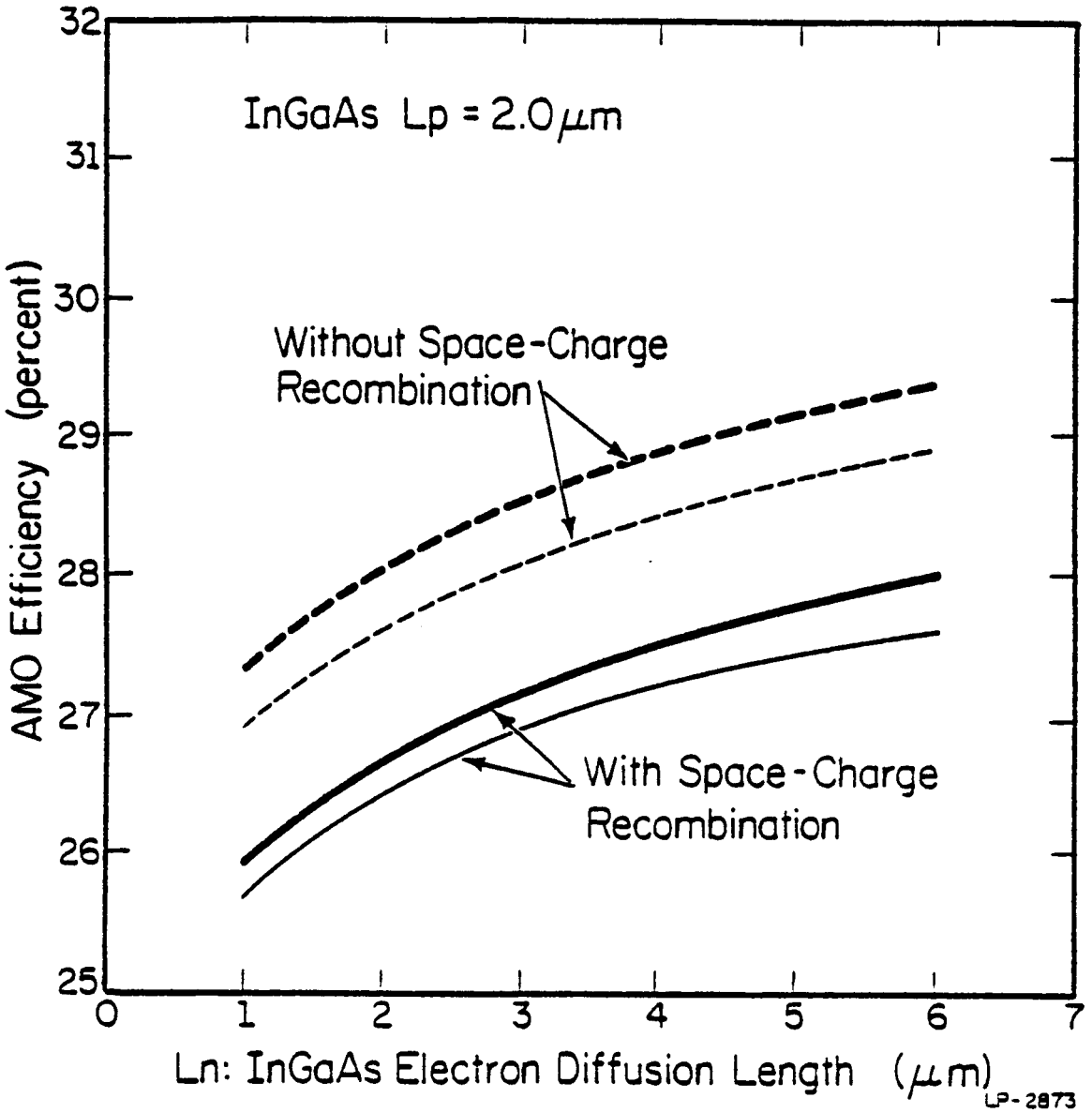

Figure 11. Beginning-of-life efficiencies of the six-layer (thick lines) and five-layer (thin lines) two-terminal AlGaAs-InGaAs MJSCs with ideal IOCs as a function of InGaAs electron diffusion length under one-sun AMO illumination (L_p = 2.0 μm, T = 300 K). These two-terminal MJSCs provide a good estimate of the performance potential of the complementary configuration. The dashed curves represent efficiencies that would be obtained if space-charge recombination were suppressed.

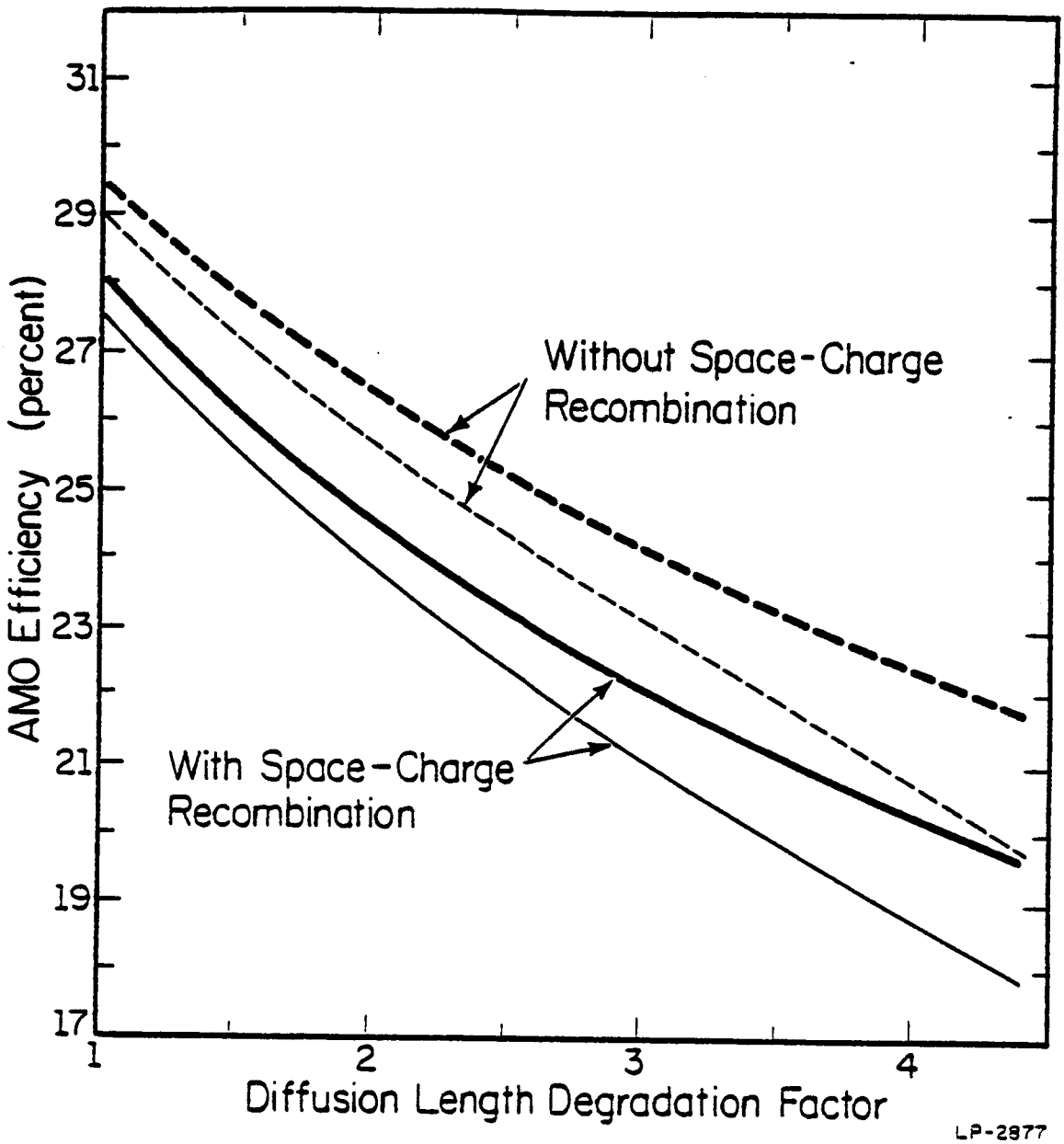

Figure 12. Effects of radiation damage on six-layer (thick lines) and five-layer (thin lines) two-terminal AlGaAs-InGaAs MJSCs with ideal IOCs. These MJSCs provide a good estimate of the performance potential of the complementary configuration.

efficiency of 75% of the BOL efficiency and uniform deterioration of diffusion lengths with time, the six-layer MJSC will last about 17% longer than the five-layer MJSC.

5. CONCLUSIONS

An alternative class of photovoltaics has been presented, which is designed to overcome two problem areas with conventional cascade designs: poor upper subcell performance and lossy IOCs. Our study has shown that upper subcell quality can be improved by incorporating additional junctions into the upper subcell and that the problems with monolithic IOCs may be circumvented by using complementary pairs of three-terminal cells or a 1 x 2 voltage-matched configuration. Realistic simulations show that AlGaAs-GaAs and AlGaAs-InGaAs MJSCs may achieve BOL one-sun, AMO efficiencies of 26% and 28%, respectively. Complementary cells made in the AlGaAs-InGaAs system can achieve BOL one-sun AMO efficiencies in excess of 27%. Seven-layer MJSCs are most advantageous for space applications due to their superior tolerance to radiation degradation.

REFERENCES

[1] H. J. Hovel, "Solar Cells," *Semiconductors and Semimetals*, vol. 11, R. K. Willardson and A. C. Beers, Eds. New York: Academic Press, 1975.

[2] J. G. Werthen, G. F. Virshup, C. W. Ford, C. R. Lewis, and A. C. Hamaker, "21% (one-sun air mass zero) 4 cm^2 GaAs space solar cell," *Appl. Phys. Lett.*, vol. 48, pp. 74-75, 1986.

[3] C. R. Lewis, W. T. Dietze, and M. J. Ludowise, "Development of a 30 percent efficient 3-junction monolithic cascade solar cell," *Space Photovoltaic Research and Technology 1983*, Cleveland: NASA, 1983, pp. 140-147.

[4] M. F. Lamorte and D. H. Abbot, "Window losses and current-mismatch computer modelling studies in AlGaAs-GaAs cascade solar cell," *IEEE Trans. Electron Devices*, vol. ED-30, pp. 1313-1322, 1983.

[5] P. Borden,"Space environment workshop," *Space Photovoltaic Research and Technology 1982*, Cleveland: NASA, 1982, p. 261.

[6] J. A. Hutchby, R. J. Markunas, M. L. Timmons, P. K. Chaing, and S. M. Bedair, "A review of multijunction concentrator solar cells," *Proceedings of the 18th IEEE Photovoltaic Specialists Conference*. New York: IEEE, 1985, pp. 20-27.

[7] C. R. Lewis, C. W. Ford, G. F. Virshup, B. A. Arua, R. T. Green, and J. G. Werther, "A two-terminal, two-junction monolithic cascade solar cell in a lattice-mismatched system," *Proceedings of the 18th IEEE Photovoltaic Specialists Conference*. New York: IEEE, 1985, pp. 556-561.

[8] M. Wagner and J. P. Leburton, "Proposal for superstructure-based high-efficiency photovoltaics," *Appl. Phys. Lett.*, vol. 49, pp. 886-888, 1986.

[9] F. Capasso, "The channeling avalanche photodiode: a novel ultra-low-noise interdigitated p-n junction detector," *IEEE Trans. Electron Devices*, vol. ED-29, pp. 1388-1393, 1982.

[10] G. H. Dohler, G. Hasnain, and J. N. Miller, "In situ grown-in selective contacts to n-i-p-i doping superlattice crystals using molecular beam epitaxial growth through a shadow mask," *Appl. Phys. Lett.*, vol. 49, 1986, p. 704.

[11] J. C. C. Fan, B-Y. Tsaur, and B. J. Palm, "Optimal design of high-efficiency tandem cells," *Proceedings of the 16th IEEE Photovoltaic Specialists Conference*. New York: IEEE, 1982, p. 692.

[12] S. Sakia, and M. Umeno, "Theoretical analysis of new wavelength-division solar cells," *J. Appl. Phys.*, vol. 51, 1980, p. 5018.

[13] J. M. Gee, "Voltage-matched configurations for multijunction solar cells," *Proceedings of the 19th IEEE Photovoltaic Specialists*. New York: IEEE, (in press).

[14] H. J. Hovel, "The effect of depletion region recombination currents on the efficiencies of Si and GaAs solar cells," *Proceedings of the 10th IEEE Photovoltaic Specialists Conference*. New York: IEEE, 1973, pp. 34-39.

[15] H. J. Hovel and J. M. Woodall, "Theoretical and experimental evaluations of $Ga_{1-x}Al_xAs$-GaAs solar cells," *Proceedings of the 10th IEEE Photovoltaic Specialists Conference*. New York: IEEE, 1973, p. 25.

[16] K. Mitsui, S. Yushida, T. Oda, M. Kato, Y. Yukimoto, and S. Matsuda, "A high quality AR coating for AlGaAl/GaAs solar cells," *Proceedings of the 17th IEEE Photovoltaic Specialists Conference*. New York: IEEE, 1984, p. 106.

[17] J. A. Hutchby and R. L. Fudurich, "Theoretical analysis of AlGaAs-GaAs graded band-gap solar cells," *J. Appl. Phys.*, vol. 47, pp. 3140-3151, 1976.

[18] H. H. Rosenbrock, "An automatic method for finding the greatest or least value of a function," *Comp. J.*, vol. 3, p. 175, 1960.

[19] M. J. Chen and C-Y. Wu, "A new method for computer-aided optimization of solar cell structures," *Solid-State Electron.*, vol. 28, p. 751, 1968.

[20] S. C. Choo, "Carrier generation-recombination in the space-charge region of an asymmetrical p-n junction," *Solid-State Electron.*, vol. 11, p. 1069, 1968.

[21] C. E. Backus, Ed., *Solar Cells*. New York: IEEE, 1976, p. 2.

[22] M. P. Godlewski, C. R. Baraona, and H. W. Brandhorst, "Low-high junction theory applied to solar cells," *Proceedings of the 10th IEEE Photovoltaic Specialists Conference*. New York: IEEE, 1973, pp. 40-49.

[23] C. Goradia and M. Challa-Goradia, "Near optimum design of GaAs-based concentrator space solar cell for 80C° operation," *Proceedings of the 17th IEEE Photovoltaic Specialists Conference*. New York: IEEE, 1984, pp. 56-62.

[24] J. E. Sutherland and J. R. Hauser, "A computer analysis of heterojunction and graded composition solar cells," *IEEE Trans. Electron Devices*, vol. ED-24, pp. 363-372, 1977.

[25] M. F. Lamorte and D. H. Abbott, "Computer modeling of a two-junction monolithic cascade solar cell," *IEEE Trans. Electron Devices*, vol. ED-27, pp. 231-249, 1980.

[26] J. L. Educato, M. Wagner, and J. P. Leburton, "AlGaAs-InGaAs SHEP's for space applications," *Proceedings of the 19th IEEE Photovoltaic Specialists Conference*. New York: IEEE, (in press).